MOLECULAR IMAGING AND BIOLOGY

Mol Imaging Biol (2019) 21:183–190
DOI: 10.1007/s11307-018-1225-8

Published Online: 12 June 2018

RESEARCH ARTICLE

Metabolic Imaging Phenotype Using Radiomics of [^{18}F]FDG PET/CT Associated with Genetic Alterations of Colorectal Cancer

Shang-Wen Chen,[1,2,3] Wei-Chih Shen,[4] William Tzu-Liang Chen,[2,5] Te-Chun Hsieh,[6,7] Kuo-Yang Yen,[6,7] Jan-Gowth Chang,[2,8] Chia-Hung Kao[2,6,9]

[1]*Department of Radiation Oncology, China Medical University Hospital, Taichung, Taiwan*
[2]*Graduate Institute of Clinical Medical Science, School of Medicine, College of Medicine, China Medical University, No. 2, Yuh-Der Road, Taichung, 404, Taiwan*
[3]*Department of Radiology, School of Medicine, Taipei Medical University, Taipei, Taiwan*
[4]*Department of Computer Science and Information Engineering, Asia University, Taichung, Taiwan*
[5]*Department of Surgery, China Medical University Hospital, Taichung, Taiwan*
[6]*Department of Nuclear Medicine and PET Center, China Medical University Hospital, Taichung, Taiwan*
[7]*Department of Biomedical Imaging and Radiological Science, China Medical University, Taichung, Taiwan*
[8]*Department of Laboratory Medicine, Chine Medical University Hospital, Taichung, Taiwan*
[9]*Department of Bioinformatics and Medical Engineering, Asia University, Taichung, Taiwan*

Abstract

Purpose: To understand the association between genetic mutations and radiomics of 2-deoxy-2-[^{18}F]fluoro-D-glucose ([^{18}F]FDG) positron emission tomography (PET)/x-ray computed tomography (CT) in patients with colorectal cancer (CRC).

Procedures: This study included 74 CRC patients who had undergone preoperative [^{18}F]FDG PET/CT. A total of 65 PET/CT-related features including intensity, volume-based, histogram, and textural features were calculated. High-resolution melting methods were used for genetic mutation analysis.

Results: Genetic mutants were found in 21 *KRAS* tumors (28 %), 31 *TP53* tumors (42 %), and 17 *APC* tumors (23 %). Tumors with a mutated *KRAS* had an increased value at the 25th percentile of maximal standardized uptake value (SUV_{max}) within their metabolic tumor volume (MTV) ($P < .0001$; odds ratio [OR] 1.99; 95 % confidence interval [CI] 1.37–2.90) and their contrast from the gray-level cooccurrence matrix ($P = .005$; OR 1.52; 95 % CI 1.14–2.04). A mutated *TP53* was associated with an increased value of short-run low gray-level emphasis derived from the gray-level run length matrix ($P = .001$; OR 243006.0; 95 % CI 59.2–996,872,313). *APC* mutants exhibited lower low gray-level zone emphasis derived from the gray-level zone length matrix ($P = .006$; $OR < .0001$; 95 % CI 0.000–0.22).

Conclusion: PET/CT-derived radiomics can provide supplemental information to determine *KRAS*, *TP53*, and *APC* genetic alterations in CRC.

Key words: Positron emission tomography computed tomography (PET/CT), Colorectal cancer (CRC), Radiomics, Mutations

Shang-Wen Chen, Wei-Chih Shen, Jan-Gowth Chang and Chia-Hung Kao contributed equally to this work.

Electronic supplementary material The online version of this article (https://doi.org/10.1007/s11307-018-1225-8) contains supplementary material, which is available to authorized users.

Correspondence to: Chia-Hung Kao; *e-mail:* d10040@mail.cmuh.org.tw

Introduction

Colorectal cancer (CRC) is the third most commonly occurring malignancy worldwide [1]. Recently derived molecular information has provided new insights into its carcinogenesis and early detection mechanisms and prognostic markers of effective drug therapy for CRC. The common somatic mutations in CRC are *KRAS*, *TP53*, and adenomatous polyposis coli (*APC*), which contribute to colorectal carcinogenesis [2, 3]. In addition, mutations of these genomes have been indicated as prognostic factors of CRC, and patients with *KRAS* mutations have been demonstrated to have therapeutic implication in CRC [3–7].

Currently, 2-deoxy-2-[^{18}F]fluoro-D-glucose ([^{18}F]FDG) positron emission tomography (PET) imaging is widely used for initial staging, evaluation of disease recurrence, and monitoring the treatment response of CRC. Several studies have explored the association between genetic alterations and [^{18}F]FDG-PET in CRC but have obtained conflicting results [8–12]. We previously revealed that mutated *KRAS* tumors are associated with higher values by using a 40 % threshold level for the maximal uptake of tumor width, whereas mutated *TP53* tumors have an increased maximal standardized uptake value (SUV_{max}) [9]. However, additional studies are required due to the low predictive accuracy. Recently, radiomics has become an increasingly widely applied approach for investigating intra-tumoral heterogeneity and its role in the proliferation, vascular supply, and metabolism of various solid malignancies [13]. The uptake heterogeneity observed within tumors assayed through [^{18}F]FDG-PET may provide not only prognostic value but also certain imaging phenotypes associated with specific genetic alterations. However, to date, there is a paucity of studies evaluating the correlation between imaging phenotypes by using radiomics and genotypes of CRC. Given that somatic mutations can change the ability of cancer cells to grow in unregulated conditions, our hypothesis is that an imaging phenotype measured quantitatively through radiomics can reflect the CRC genotype.

Although mutation analysis of tumor tissues remains a standard-of-care assessment, imaging studies can provide additional information if biopsies fail to be performed. Therefore, in this pilot study, we aimed to determine the most effective approach for quantitatively measuring an imaging phenotype through radiomics to distinguish mutant and wild-type genomes in CRC. The results might supplement the mutational status to intensify the optimal therapeutic strategies for CRC patients.

Materials and Methods

Patient Population

This retrospective study included 103 newly diagnosed CRC patients scheduled to undergo curative surgical procedures at China Medical University Hospital between January 2009 and December 2012. Patients receiving neoadjuvant chemoradiotherapy or chemotherapy were not under the scope of this study because small amounts of tumor tissues from biopsy specimens were insufficient to fit the requirement of our genetic analysis.

Genetic Mutation Analysis

A routine pathology examination was performed following tumor resection, and the tumor and normal tissues were preserved in a tissue bank at China Medical University Hospital.

High-resolution melting (HRM) methods were used for genetic mutation analysis. An effective amplicon design is essential to obtain robust and reproducible HRM analysis. The distinction between wild-type and heterozygote curves becomes smaller and more difficult when the product length increases; therefore, it has been suggested that all amplicons should be designed to be smaller than 300 bp. In the present study, the primers for HRM analysis were selected using Primer3 software.

For the amplification of the *APC* gene, polymerase chain reaction (PCR) was performed in duplicate in a volume of 10 μl with a LightCycler 480 HRM Master (Reference 04909631001, Roche Diagnostics) by using a 1× buffer containing Taq polymerase, nucleotides, the dye ResoLight, 10 ng DNA, 0.3 μM primers, and 2.5 mM $MgCl_2$. In addition, analyses of the *TP53*, *PIK3CA*, *KRAS*, and *BRAF* genes were performed in a volume of 15 μl with a Type-it HRM PCR Kit (Qiagen, Hilden, Germany) by using a 1× HRM PCR master mix containing HotStar Taq Plus DNA polymerase, Type-it HRM PCR buffer, Q-solution, dNTP and EVA green dye, and 15 ng DNA, as well as 0.66 μM each of *TP53* and *BRAF* gene primers, and 0.67 μM each of *PIK3CA* and *KRAS* gene primers. HRM assays were analyzed using commercial software (LightCycler 480 Gene Scanning Software Version 1.5, Roche Diagnostics). This procedure is detailed in our previously published work [9, 14].

PET/CT Image Acquisition

All patients received PET/CT for pretreatment staging and underwent primary tumor resection thereafter (median: 7 days; range: 1–28 days). All patients fasted for at least 4 h prior to [^{18}F]FDG PET/CT imaging to minimize the impact of serum glucose level on acquired images. The images were captured using a PET/CT scanner (PET/CT-16 slice, Discovery STE, GE Medical System, Milwaukee, WI, USA) approximately 60 min after patients were administered 370 MBq of [^{18}F]FDG. A topogram was performed to define the scan range, followed by a non-contrast-enhanced low-dose CT scan (0.8 s tube rotation, 120 kVp, AutomA, 3.75 mm slice thickness and a pitch of 1.75) used for anatomical localization and attenuation correction. PET studies were scanned in three-dimensional (3D) acquisition mode with 2 min per bed position and 11-slice overlap of bed positions. The images were reconstructed using 3D ordered subset expectation maximization algorithms (OSEM, 20 iterations, 2 subsets). A 3-mm-full width at half maximum (FWHM) Gaussian filter was applied after the reconstruction. The matrix size was 128 voxels × 128 voxels × length of interest, whereas the voxel size was 5.47 mm × 5.47 mm × 3.27 mm.

The [^{18}F]FDG-PET data were inputted into the workstation (Advantage Workstation Ver. 4.4, GE Healthcare), and the images were reviewed to localize the target lesions. The results were confirmed by two nuclear medicine physicians who were unaware of the information in the preoperative images. The PET/CT workstation provided a quantification of [^{18}F]FDG uptake for SUV. The nuclear medicine physicians identified the locations of SUV_{max} and the values for the primary tumors. This procedure is detailed in our previous report [9]. Among the 103 patients included for genetic analyses, 29 patients without intravenous furosemide (20 mg) administration before image acquisition were excluded. The rationale was to avoid the bias of diuretics on image extraction. In total, radiomics extraction was successfully retrieved in 74 patients. Tumor locations were colon or sigmoid colon (40 patients) and rectum or rectosigmoid junction (34 patients). The median age was 58 years (range: 26–85 years), 46 of patients were men, and 28 were women. The characteristics of all 74 patients are shown in Table 1.

Extraction of the Radiomic Features of Colorectal Tumors

The voxel within the volume data of a PET image series was defined as a local maximum if its SUV was not less than those of its 18 neighboring voxels. The SUV_{max} of a colorectal tumor was the local maximum with the largest SUV within the spatial extent. The metabolic tumor volume (MTV) was further delineated using a relative threshold of SUV_{max}, which was defined as $SUV_{max} \times 0.5$ and was used to delineate the MTVs of 70 colorectal tumors [15]. Because the MTV was too small to evaluate radiomic features, the threshold was adjusted to $SUV_{max} \times 0.4$ for four tumors. For every MTV, a total of 63 radiomic features were derived from the SUVs of MTV (Table S1 in Electronic Supplementary Material (ESM)), including 7 conventional features (SUV_{max}, SUV_{peak}, SUV_{total}, MTV, TLG_{max}, TLG_{peak}, and TLG_{mean}); 8 histogram-based features (mean, variance, standard deviation, skewness, kurtosis, 25th percentile, median, and 75th percentile); and 48 textural features. A total of 21 3D texture features were derived from the gray-level cooccurrence matrix (GLCM) [16], 5 from the neighborhood gray-level different matrix (NGLDM) [17], 11 from the gray-level run length matrix (GLRLM) [18], and 11 from the gray-level zone length matrix (GLSZM) [19]. Before constructing the four matrices, the SUVs within an MTV were discretized by a bin width of 1.75 g/ml for constructing GLCM, NGLDM, and GLRLM and by a bin width of 1 g/ml for constructing GLSZM. The construction of GLCM or GLRLM depends on a direction parameter. Therefore, to summarize the evaluations of 13 possible directions, the maximum and minimum measurements were adopted for every textural feature defined in GLCM and GLRLM. The correlation between the radiomic features and MTVs is listed in Table S2 (in ESM).

Table 1. Patients' characteristic ($N = 74$)

Characteristic	Value
Age (years)	26–85 (median, 58)
Gender	Male: 46, female: 28
Primary lesion location	
Colon or sigmoid colon	40
Rectum or rectosigmoid junction	34
CEA (ng/dl)	38.5 ± 133.3 (0.5–959.5)
Pathological staging (AJCC 7th ed.)	
T stage	T1–2:13, T3:50, T4:11
N stage	N0:36, N1:15; N2: 23
M stage	M0:41,M1:33
Differentiation	
W-D	5
M-D	63
P-D	6
P53	
Mutant	31
Wild-type	43
KRAS	
Mutant	21
Wild-type	53
APC	
Mutant	17
Wild-type	57
SUV_{max}	14.6 ± 8.0 (3.8–42.3)
MTV	15.5 ± 19.1 (1.9–63.5)
TLG_{mean}	152.7 ± 145.6 (12.4–707.3)

ECOG Eastern Cooperation Oncology Group, *AJCC* American Joint Committee on Cancer, *CEA* carcinoembryonic antigen, *W-D* well-differentiation, *M-D* moderate differentiation, *P-D* poor differentiation, *MTV* metabolic tumor volume, TLG_{mean} total total lesion glycolysis

Statistical Analysis

All values are expressed as mean ± standard deviation. To compare the predictive ability for genetic mutants, all extracted features were first examined using receiver-operating characteristic (ROC) curve analysis. The predictive abilities for the mutational status were compared using the area under the curve (AUC). If the AUC for any feature was above 0.6 or below 0.4, the quantitative differences in these indices between mutated and wild-type genomes were examined using the Mann–Whitney *U* test. To minimize the risk of statistical type 1 errors, one-way ANOVA *post hoc* Bonferroni test was utilized to confirm the statistical tests. Thereafter, all statistically significant textural indices combined with conventional PET/CT and clinical parameters were tested using binary logistic regression analysis to identify the most predictable factors for specific genetic mutations. All analyses were two-sided, with $P < .05$ considered statistically significant. For statistically significant textural features associated with the presence of mutations, we determined the optimal cutoff by maximizing the couple sensibility/specificity by using ROC analysis. Correlations between different genomic alterations or PET/CT-related features were tested examined using Spearman's rank correlation coefficient, with the alpha level set at 0.01. Statistical analyses were performed using SPSS version 16.0 (SPSS Inc., Chicago, IL, USA).

Results

Frequency of Genetic Alterations

As shown in Table 1, genetic alterations in *KRAS* (codons 12 and 13), *TP53* (exons 2–11), and *APC* were, respectively, identified in 21 (28 %), 31 (42 %), and 17 (23 %) patients. The mutants in *PIK3CA* and *BRAF* were identified in two (3 %) and three (4 %) patients, respectively. In seven patients (9 %), our data showed that *TP53* and *KRAS* mutations coexisted in the same tumors. Nineteen (26 %) had no any mutations mentioned above. In addition, no obvious correlation was observed between the two genetic mutants *(*$P = 0.35$, $\gamma = -0.11$*)*. Similarly, no associations were observed between *TP53* and *APC* mutants *(*$P = 0.54$, $\gamma = -0.07$*)* or between *KRAS* and *APC* mutants ($P = 0.48$, $\gamma = 0.08$). Because of the rarity of genetic alterations in *PIK3CA* and *BRAF*, these genes were excluded from the analysis.

Predictive Value of PET/CT-Related Features for the KRAS Mutation

In addition to SUV_{max}, the Mann–Whitney *U* test revealed that 6 histogram and 40 textural indices showed predictive values for mutated *versus* wild-type *KRAS*. The quantitative differences are listed in Table S3 (in ESM). As summarized in Table 2, the logistic regression analysis showed that Prctile25 in the histograms and contrast from GLCM were two independent predictors of the *KRAS* mutation. The odds ratio (OR) was 1.99 ($P \leq .0001$; 95 % confidence interval [CI] 1.37–2.90) and 1.52 ($P = .005$; 95 % CI 1.14–2.04), respectively. Figure 1 depicts the quantitative difference in Prctile25 and contrast between the two groups, as well as the corresponding ROC curves. The mean value of Prctile25 for patients with and without mutations was 11.4 ± 4.9 and 7.1 ± 3.7 ($P < .001$), whereas that of contrast for those with and without mutations was 6.0 ± 6.4 and 3.1 ± 4.6 cm ($P = .002$), respectively.

Table 2. Result of logistic regression analyses and estimating odds ratios of for predicting *KRAS* mutation

Variables	Univariate *p* value	Multivariate *p* value	OR	95 % CI
Age	0.11	0.27	1.01	0.97–1.07
pT1–2 *vs.* pT3–4	0.62	0.96	1.35	0.08–7.45
pN0 *vs.* pN 1–3	0.17	0.53	1.33	0.19–2.99
CEA level (ng/dl)	0.42	0.62	1.00	0.99–1.01
SUVmax	< 0.0001	0.83	1.05	0.45–2.01
MTV (ml)	0.93	0.62	1.00	1.00–1.00
TLG_{mean} (g)	0.06	0.36	0.99	0.98–1.01
Prctile25	< 0.0001	< 0.0001	1.99	1.37–2.90
Contrast (GLCM)	0.04	0.005	1.52	1.14–2.04

OR odds ratio, *CI* confidence interval, *CEA* carcinoembryonic antigen, *SUVmax* maximal standard uptake value of the primary tumor, *MTV* metabolic tumor volume, TLG_{mean} total lesion glycolysis, *Prctile25* the 25th percentile is a measurement of relative standing within SUVs of a MTV, *GLCM* gray level cooccurrence matrix

Predictive Value of PET/CT-Related Features for the TP53 Mutation

According to Mann–Whitney *U* test results, compared with wild-type *TP53*, only mutated *TP53* CRC tumors were found to be associated with an increased short-run low gray-level emphasis (SRLGE) derived from GLRLM (Table S4 in ESM). The AUC for predicting *TP53* was 0.71 ($P = 0.002$). As summarized in Table 3, logistic regression analysis revealed that SRLGE was the only predictor of *TP53* mutations, with an OR of 243,006.0 ($P = .001$; 95 % CI 59.2–996,872,313). The quantitative difference in the SRLGE between the two groups is illustrated in Fig. 2. The mean SRLGE for patients with and without *TP53* mutations was 0.38 ± 0.07 and 0.33 ± 0.08 ($P = .003$), respectively. Furthermore, none of the radiomics, conventional, or histogram-based parameters, or clinical variables was associated with tumors with simultaneous presence of *TP53* and *KRAS* mutations.

Predictive Value of PET/CT-Related Features for the APC Mutation

The ROC curves and the Mann–Whitney *U* test revealed that the lower low gray-level zone emphasis (LGZE) derived from GLSZM was the only predictor of the *APC* mutant (Table S5 in ESM). As listed in Table 4, in the multivariate analysis, mutated *APC* CRC tumors tended to be associated with a decreased LGZE ($P = .006$; OR < .0001; 95 % CI 0.000–0.22). The mean LGZE values for patients with and without mutations were 0.29 ± 0.09 and 0.35 ± 0.11 ($P = .03$), respectively (Fig. 3).

Accuracy in Predicting Genetic Alteration

Based on the parameters for the *KRAS* and *TP53* mutations mentioned earlier, we sought to determine the optimal cutoffs for distinguishing between the mutant and wild-type genomes. When using an optimal cutoff value of 7.5 for Prctile25, the corresponding sensitivity, specificity, and accuracy for predicting the *KRAS* mutation were 76, 74, and 74 %. When using a cutoff of 2.0 for contrast, the corresponding values were 76, 60, and 65 %. When combining the two indices, sensitivity, specificity, and accuracy reached 81, 74, and 77 %, respectively. For the *TP53* mutation, when using an optimal cutoff of 0.32 for SRLGE, sensitivity, specificity, and accuracy were 84, 47, and 62 %, respectively.

Differences of Textural Features Between Rectal and Colon Tumors

Using the Mann–Whitney *U* test or logistic regression analysis, there was no difference of textural features or genetic mutations between rectal and colon tumors.

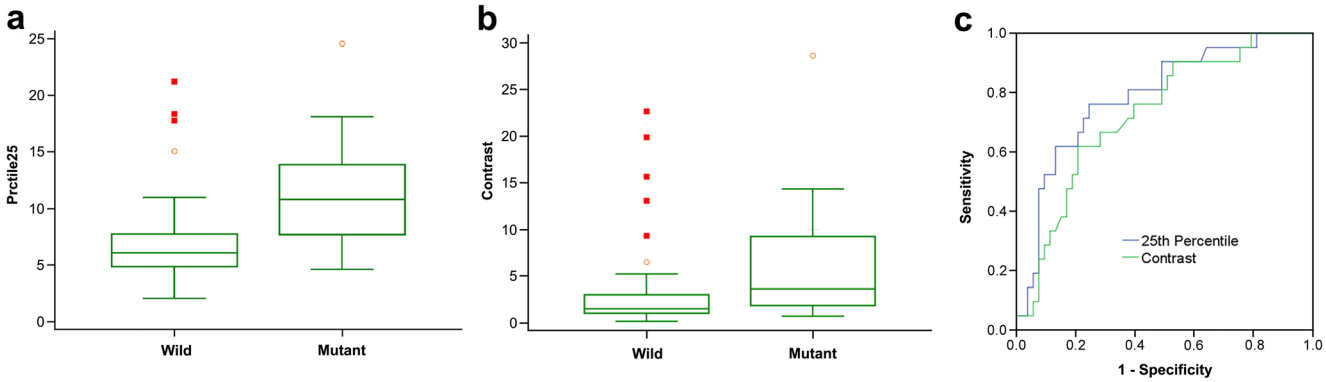

Fig. 1. *KRAS* mutant associated with quantitative values of textural features: **a** Prctile25, **b** contrast, **c** receiver-operating characteristic (ROC) curves. The areas under the curve for Prctile25 and contrast were 0.79 ± 0.06 ($P < .0001$) and 0.73 ± 0.06 ($P = .0002$), respectively.

Discussion

Because the mutational sequence obtained from biopsies usually quantifies a small part of potentially heterogeneous tumors, sometimes repeat tumor sampling might be impractical. Therefore, the radiomic signature related to tumor heterogeneity, combined with clinical data, has great implications for imaging-based biomarkers in the clinical settings [20]. Although the mechanisms underlying [^{18}F]FDG accumulation in cancer tissues are complex, a unique advantage of radiomics of a [^{18}F]FDG-PET scan is the ability to use the quantitative information of the glucose uptake and distribution within the tumor. By testing numerous discretization methods and using comprehensive textural features, this pilot study provides a basis through which [^{18}F]FDG PET/CT scans can be considered predictive of the macroscopic mutational status of the whole tumor. This information can be used to decide the therapeutic strategy.

The stability and robustness of extracted radiomics improve the reproducibility of this study. Conventional texture analyses are challenging [13, 15] because the different discretization methods and adjustable parameters introduce incoherent texture feature extraction and lead to nonrobust diagnostic capability. We hypothesized that the extracted textural features would be stable and robust if its measurements for an MTV indicated high consistency under different parameters of a discretization method. Two methods, a fixed number of bins or a fixed bin width, were used with different parameter settings to discretize the SUVs within an MTV. For each radiomics, exploratory factor analysis with various rotation was conducted to investigate the relationships among the measurements of all MTVs under different parameter settings. The underlying structure of all possible parameter settings was therefore decomposed into several factors, each corresponding to a set of parameter settings of a discretization method. Based on the requirement of predicting the mutation of *KRAS*, *TP53*, and *APC*, the ability of the axis of a factor was evaluated through ROC curve analysis and decided the selection of the discretization method and parameter settings. Thus, the identified textural feature was stable and robust. Because the focus of this study was the ability of features to predict mutations, the details of feature selection will be discussed in other work.

The oncogenic activation of *KRAS* can influence several cellular processes that regulate biological mechanisms [21]. Increased glucose transport and glycolysis have been observed

Table 3. Result of logistic regression analyses and estimating odds ratios of for predicting *TP53* mutation

Variables	Univariate *p* value	Multivariate *p* value	OR	95 % CI
Age	0.80	0.97	0.99	0.95–1.04
pT1–2 *vs.* pT3–4	0.35	0.37	1.47	0.27–8.02
pN0 *vs.* pN 1–3	0.12	0.21	2.10	0.61–7.27
CEA level (ng/dl)	0.31	0.71	1.00	0.99–1.01
SUVmax	0.88	0.10	1.12	0.98–1.29
MTV (ml)	0.42	0.16	1.00	1.00–1.00
TLG_{mean} (g)	0.40	0.12	1.00	1.00–1.00
SRLGE	0.009	0.001	243,006.0	59.2–996,872,313

Abbreviations: as Table 2; *SRLGE* short-run low gray-level emphasis

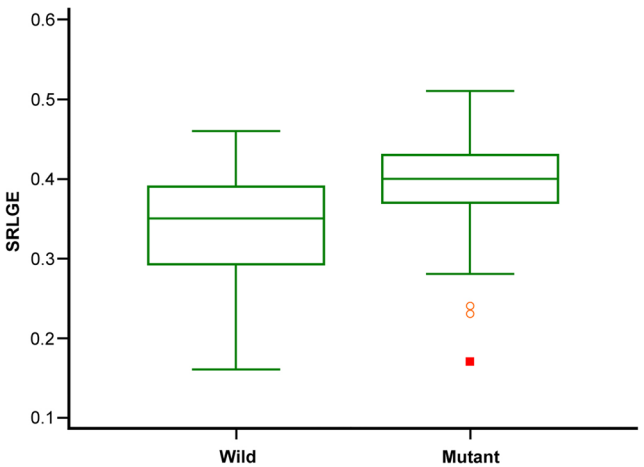

Fig. 2. *TP53* mutant associated with quantitative values of short-run low gray-level emphasis (SRLGE).

Table 4. Result of logistic regression analyses and estimating odds ratios for predicting *APC* mutation

Variables	Univariate *p* value	Multivariate *p* value	OR	95 % CI
Age	0.99	0.81	1.01	0.96–1.06
pT1–2 *vs.* pT3–4	0.45	0.60	2.84	0.33–24.19
pN0 *vs.* pN 1–3	0.63	0.76	1.05	0.28–3.92
CEA level (ng/dl)	0.73	0.27	0.99	0.97–1.01
SUVmax	0.45	0.08	0.83	0.69–1.01
MTV (ml)	0.22	0.61	1.00	1.00–1.00
TLG_{mean} (g)	0.96	0.72	1.01	0.99–1.01
LGZE	0.023	0.006	< .0001	0.000–0.22

Abbreviations: as Table 2; *LGZE* low gray-level zone emphasis

in KRAS-mutated colorectal or pancreatic cancer cell lines [22]. The negative predictive role of *KRAS* mutation is particularly crucial for CRC because it can predict a lack of response to therapies with antibodies targeted to the epidermal growth factor receptor [4, 5]. The American Society of Clinical Oncology suggests that patients with metastatic CRC who have a *KRAS* mutation in codon 12 or 13 should not receive antiepidermal growth factor receptor antibody treatment [23]. This study provides evidence that several histogram indices and textural features of [^{18}F]FDG-PET are predictive of mutated *KRAS*. Furthermore, when two features were combined, namely Prctile25 or contrast (GLCM) (AUC = 0.79 and 0.73, respectively), sensitivity and accuracy reached 81 and 77 %. The values can provide more information on the *KRAS* status than that reported by previous studies [8–10].

Kawada et al. conducted a pilot study by using SUV_{max} in a cohort of 51 CRC patients [8], and they showed that SUV_{max} had an OR of 1.17 with an accuracy of 75 % in predicting mutated *KRAS* when using a cutoff of 13. Lovinfosse et al. investigated a cohort of 151 rectal cancer patients and found that both the SUV coefficient of variation (SUVcov) and SUV_{max} exhibited an AUC of 0.65 with respective sensitivities of 56 and 69 % and specificities of 64 and 52 % [10]. In their study; however, the contrast (GLCM) was not capable of predicting mutated *KRAS*. In addition, the calculated values were higher than ours. The

Fig. 3. *APC* mutant associated with quantitative values of low gray-level zone emphasis (LGZE).

disparities between two studies might be attributed to different technical approaches, such as definition of MTV or discretization method. Particularly, the selection of the discretization affects the quantization results and transforms the performance of the radiomics. Nonetheless, we assume that CRC tumors with mutated *KRAS* are associated with increased [^{18}F]FDG uptake or heterogeneous distribution. However, whether the underlying molecular mechanism driving this process is always reproducible in [^{18}F]FDG-PET across various cancers must be clarified, because one large cohort study investigating PET-based radiomics in non-small-cell cancer patients suggested that *KRAS* mutations do not guide different metabolic imaging phenotypes [24]. Nonetheless, if the imaging signature suggests a different *KRAS* status compared with previous tissue assessment, this suggests rebiopsy of the target lesions to maximize the therapeutic effect.

In CRC tumorigenesis, *TP53* and *KRAS* mutations play a role in separate pathways [3]. The clinical significance of the somatic mutations in *TP53* remains debated in terms of survival or response to a therapy [25]. Some studies have suggested that *TP53* plays a role in modulating metabolism, including glycolysis and oxidative phosphorylation [26, 27]. Mutated *TP53* tumors may exhibit increased glucose consumption and direct glucose utilization for biosysthesis [26]. A cell line study reported that *TP53* mutant cells had 1.5–2 times the [^{18}F]FDG uptake than did wild-type *TP53* cells under the basal condition, and the difference in [^{18}F]FDG uptake was greater after Rhenium-188 treatment [28]. Although we previously indicated that mutant *TP53* tumors tended to exhibit higher SUV_{max} across several threshold methods applied for distinguishing wild-type and mutant genomes [9], newer approaches are required to overcome low sensitivity and accuracy. Through a comprehensive [^{18}F]FDG-PET radiomics signature, this study indicated that tumors with the *TP53* mutation had an increased SRLGE from GLRLM, with an AUC of 0.71 and an accuracy of 62 %. Additional studies are required to confirm this finding. Notably, abnormal FDG-PET signals can be observed in evolutionary pre-malignant CRC tumors, matching the time when *TP53* mutations appear.

Mutations in the *APC* gene are responsible for familial adenomatous polyposis and the majority of sporadic CRC cases [29]. Compared with the *KRAS* or *TP53* mutation, the *APC* mutation alone has seldom been reported as a poor prognostic factor of CRC. This study indicates a negative predictive value of LGZE for *APC* mutation; however, this must be validated by future studies due to the limited number of patients with *APC* mutants.

The findings of this study should be interpreted cautiously because they were derived from a retrospective study conducted at a single institute. The findings should be confirmed by external validation studies using various scanner manufacturers, resolution settings, and reconstruction algorithms. Second, PET/CT may represent the gross status of the tumors. The heterogeneity of the mutations within a CRC tumor might bias the correlation study because dissected specimens for mutational testing may not reflect the exact macroscopic status of the entire tumor. In addition, features derived from [^{18}F]FDG-PET/CT are still not

sufficient to replace mutational testing because predictive specificity and accuracy are not completely acceptable. To maximize their supplemental roles for mutational testing, a combination with various features or other biomarkers can be utilized as a potential approach. In addition, the optimal approach of the MTV definition should be investigated further by comparing our advanced segmentation algorithms such as contour-based or clustered-based methods [30]. Although the MTV extracted by a fixed threshold at 50 % of SUVmax could minimize the probability for the connection with the adjacent organ, this method can possibly underestimate the functional volumes [15]. Finally, the selection of the discretization method affects the quantization results and transforms the performance of the radiomics. In the future, radiomics for a special clinical outcome should be guided by machine learning processes. Although little evidence supports a straightforward correlation between textural heterogeneity and any specific underlying physiological processes or biological heterogeneity, our findings hint that future studies can clarify molecular mechanisms that may be related to the interplay between imaging phenotypes and mutational landscapes.

Conclusions

PET/CT-derived textural features can provide supplemental information to determine *KRAS*, *TP53*, and *APC* genetic alterations in CRC. Mutated *KRAS* tumors are associated with higher Prctile25 in histograms and contrast from GLCM, whereas mutated *TP53* tumors have an increased SRLGE derived from GLRLM. *APC* mutants exhibit lower LGZE. However, additional studies are required to maximize predictive accuracy.

Acknowledgments. This work was supported by grants from the Ministry of Health and Welfare, Taiwan (MOHW107-TDU-B-212-123004), China Medical University Hospital; Academia Sinica Stroke Biosignature Project (BM10701010021); MOST Clinical Trial Consortium for Stroke (MOST 106-2321-B-039-005-); Tseng-Lien Lin Foundation, Taichung, Taiwan; and Katsuzo and Kiyo Aoshima Memorial Funds, Japan, China Medical University Hospital (CRS-106-039, CRS-106-041). The funders had no role in study design, data collection and analysis, decision to publish, or preparation of the manuscript. No additional external funding was received for this study.

Authors' Contributions. All authors have contributed substantially to, and are in agreement with the content of, the manuscript: conception/design: Shang-Wen Chen, Chia-Hung Kao; provision of study materials: Chia-Hung Kao, Jan-Gowth Chang; collection and/or assembly of data: Shang-Wen Chen, Wei-Chih Shen, William Tzu-Liang Chen, Te-Chun Hsieh, Kuo-Yang Yen, Jan-Gowth Chang, Chia-Hung Kao; data analysis and interpretation: Shang-Wen Chen, Wei-Chih Shen, William Tzu-Liang Chen, Te-Chun Hsieh, Kuo-Yang Yen, Jan-Gowth Chang, Chia-Hung Kao; manuscript preparation: Shang-Wen Chen, Wei-Chih Shen, William Tzu-Liang Chen, Te-Chun Hsieh, Kuo-Yang Yen, Jan-Gowth Chang, Chia-Hung Kao; final approval of manuscript: Shang-Wen Chen, Wei-Chih Shen, William Tzu-Liang Chen, Te-Chun Hsieh, Kuo-Yang Yen, Jan-Gowth Chang, Chia-Hung Kao. The guarantor of the paper, taking responsibility for the integrity of the work as a whole, from inception to published article: Chia-Hung Kao.

Compliance with Ethical Standards. The study was approved by the local institutional review board (certificate numbers CMUH102-REC2-74 and DMR99-IRB-010-1).

Conflict of Interest

The authors declare that they have no conflict of interest.

Ethical Approval

All procedures performed in studies involving human participants were in accordance with the ethical standards of the institutional and/or national research committee and with the 1964 Helsinki declaration and its later amendments or comparable ethical standards.

Informed Consent

The IRB also specifically waived the consent requirement.

References

1. Jemal A, Bray F, Center MM, Ferlay J, Ward E, Forman D (2011) Global cancer statistics. CA Cancer J Clin 61:69–90
2. Leslie A, Pratt NR, Gillespie K, Sales M, Kernohan NM, Smith G, Wolf CR, Carey FA, Steele RJ (2003) Mutations of APC, KRS, and P53 are associated with specific chromosomal aberrations in colorectal adenocarcinomas. Cancer Res 63:4656–4661
3. Conlin A, Smith G, Carey FA, Wolf CR, Steele RJ (2005) The prognostic significance of KRAS, P53, and APC mutations in colorectal carcinoma. Gut 54:1283–1286
4. Karapetis CS, Khambata-Ford S, Jonker DJ, O'Callaghan CJ, Tu D, Tebbutt NC, Simes RJ, Chalchal H, Shapiro JD, Robitaille S, Price TJ, Shepherd L, Au HJ, Langer C, Moore MJ, Zalcberg JR (2008) KRAS mutations and benefit from cetuximab in advanced colorectal cancers. N Engl J Med 359:1757–1765
5. Lièvre A, Bachet JB, Boige V, Cayre A, le Corre D, Buc E, Ychou M, Bouché O, Landi B, Louvet C, André T, Bibeau F, Diebold MD, Rougier P, Ducreux M, Tomasic G, Emile JF, Penault-Llorca F, Laurent-Puig P (2008) KRAS mutations as an independent prognostic factor in patients with advanced colorectal cancer treated with cetuximab. J Clin Oncol 26:374–379
6. Westra JL, Schaapveld M, Hollema H, de Boer JP, Kraak MMJ, de Jong D, ter Elst A, Mulder NH, Buys CHCM, Hofstra RMW, Plukker JTM (2005) Determination of TP53 mutation is more relevant than microsatellite instability status for the prediction of disease-free survival in adjuvant treated stage III colon cancer patients. J Clin Oncol 23:5635–5643
7. Chen TH, Chang SW, Huang CC, Wang KL, Yeh KT, Liu CN, Lee H, Lin CC, Cheng YW (2013) The prognostic significance of APC gene mutation and miR-21 expression in advanced-stage colorectal cancer. Color Dis 15:1367–1374
8. Kawada K, Nakamoto Y, Kawada M, Hida K, Matsumoto T, Murakami T, Hasegawa S, Togashi K, Sakai Y (2012) Relationship between 18F-Fluorodeoxyglucose accumulation and KRAS/BRAF mutations in colorectal Cancer. Clin Cancer Res 18:1696–1703
9. Chen SW, Lin CY, Ho CM, Chang YS, Yang SF, Kao CH, Chang JG (2015) Genetic alterations in colorectal cancer have different patterns on ^{18}F-FDG PET/CT. Clin Nucl Med 40:621–626
10. Lovinfosse P, Koopmansch B, Lambert F, Jodogne S, Kustermans G, Hatt M, Visvikis D, Seidel L, Polus M, Albert A, Delvenne P, Hustinx R (2016) ^{18}F-FDG PET/CT imaging in rectal cancer: relationship with the RAS mutational status. Br J Radiol 89:20160212
11. Krikelis D, Skoura E, Kotoula V, Rondogianni P, Pianou N, Samartzis A, Xanthakis I, Fountzilas G, Datseris IE (2014) Lack of association between KRAS mutations and 18F-FDG PET/CT in caucasian metastatic colorectal cancer patients. Anticancer Res 34:2571–2579
12. Iwamoto S, Kawada K, Nakamoto Y et al (2014) Regulation of ^{18}F-fluorodeoxyglucose accumulation in colorectal cancer cells with mutated KRAS. J Nucl Med 55:2038–2044
13. Tixier F, Groves AM, Goh V, Hatt M, Ingrand P, le Rest CC, Visvikis D (2014) Correlation of intra-tumor 18F-FDG uptake heterogeneity indices with perfusion CT derived parameters in colorectal cancer. PLoS One 9:e99567
14. Er TK, Chang JG (2012) High-resolution melting: applications in genetic disorders. Clin Chim Acta 414:197–201

15. Shen WC, Chen SW, Liang JA, Hsieh TC, Yen KY, Kao CH (2017) ^{18}Fluorodeoxyglucose positron emission tomography for the textural features of cervical cancer associated with lymph node metastasis and histological type. Eur J Nucl Med Mol Imaging 44:1721–1731
16. Haralick RM, Shanmugam K, Dinstein I (1973) Textural features for image classification. IEEE Trans Syst Man Cybern 3:610–621
17. Sun C, Wee WG (1983) Neighboring gray level dependence matrix for texture classification. Comput Vis Graph Image Process 23:341–352
18. Loh H, Leu J, Luo R (1988) The analysis of natural textures using run length features. IEEE Trans Ind Electron 35:323–328
19. Thibault G, Fertil B, Navarro C et al (2009) Texture indexes and gray level size zone matrix: application to cell nuclei classification. In: 10th International Conference on Pattern Recognition and Information Processing, PRIP 2009, Minsk, Belarus, pp 140–145
20. Rios Velazquez E, Parmar C, Liu Y, Coroller TP, Cruz G, Stringfield O, Ye Z, Makrigiorgos M, Fennessy F, Mak RH, Gillies R, Quackenbush J, Aerts HJWL (2017) Somatic mutations drive distinct imaging phenotypes in lung Cancer. Cancer Res 77:3922–3930
21. Yun J, Rago C, Cheong I, Pagliarini R, Angenendt P, Rajagopalan H, Schmidt K, Willson JKV, Markowitz S, Zhou S, Diaz LA, Velculescu VE, Lengauer C, Kinzler KW, Vogelstein B, Papadopoulos N (2009) Glucose deprivation contributes to the development of KRAS pathway mutations in tumor cells. Science 325:1555–1559
22. Ying H, Kimmelman AC, Lyssiotis CA, Hua S, Chu GC, Fletcher-Sananikone E, Locasale JW, Son J, Zhang H, Coloff JL, Yan H, Wang W, Chen S, Viale A, Zheng H, Paik JH, Lim C, Guimaraes AR, Martin ES, Chang J, Hezel AF, Perry SR, Hu J, Gan B, Xiao Y, Asara JM, Weissleder R, Wang YA, Chin L, Cantley LC, DePinho RA (2012) Oncogenic Kras maintains pancreatic tumors through regulation of anabolic glucose metabolism. Cell 149:656–670
23. Allegra CJ, Jessup JM, Somerfield MR, Hamilton SR, Hammond EH, Hayes DF, McAllister PK, Morton RF, Schilsky RL (2009) American Society of Clinical Oncology provisional clinical opinion: testing for KRAS gene mutations in patients with metastatic colorectal carcinoma to predict response to anti-epidermal growth factor receptor monoclonal antibody therapy. J Clin Oncol 27:2091–2096
24. Yip SS, Kim J, Coroller TP et al (2017) Associations between somatic mutations and metabolic imaging phenotypes in non-small cell lung cancer. J Nucl Med 58:569–576
25. Munro AJ, Lain S, Lane DP (2005) P53 abnormalities and outcomes in colorectal cancer: a systematic review. Br J Cancer 92:434–444
26. Jiang P, Du W, Wang X et al (2011) p53 regulates biosynthesis through direct inactivation of glucose-6-phosphate dehydrogenase. Nat Cell Biol 13:310–316
27. Vousden KH, Ryan KM (2009) p53 and metabolism. Nat Rev Cancer 9:691–700
28. Cheon GJ, Chung HK, Choi JA, Lee SJ, Ahn SH, Lee TS, Choi CW, Lim SM (2007) Cellular metabolic responses of PET radiotracers to ^{188}Re radiation in an MCF7 cell line containing dominant-negative mutant P53. Nucl Med Biol 34:425–432
29. Fodde R, Smits R, Clevers H (2001) APC, signal transduction and genetic instability in colorectal cancer. Nat Rev Cancer 1:55–67
30. Hatt M, Tixier F, Pierce L, Kinahan PE, le Rest CC, Visvikis D (2017) Characterization of PET/CT images using texture analysis: the past, the present… any future? Eur J Nucl Med Mol Imaging 44:151–165